IVYSPRING INTERNATIONAL PUBLISHER

Theranostics

2018; 8(10): 2696-2708. doi: 10.7150/thno.23686

Research Paper

A large, switchable optical clearing skull window for cerebrovascular imaging

Chao Zhang[1,2], Wei Feng[1,2], Yanjie Zhao[1,2], Tingting Yu[1,2], Pengcheng Li[1,2], Tonghui Xu[1,2], Qingming Luo[1,2], Dan Zhu[1,2]✉

1. Britton Chance Center for Biomedical Photonics, Wuhan National Laboratory for Optoelectronics-Huazhong University of Science and Technology, Wuhan, Hubei 430074, China
2. MoE Key Laboratory for Biomedical Photonics, Collaborative Innovation Center for Biomedical Engineering, School of Engineering Sciences, Huazhong University of Science and Technology, Wuhan, Hubei 430074, China

✉ Corresponding author: Dan Zhu, Britton Chance Center for Biomedical Photonics, Wuhan National Laboratory for Optoelectronics, Huazhong University of Science and Technology, Wuhan 430074, China. Tel: 86-027-87792033; E-mail: dawnzh@mail.hust.edu.cn.

Received: 2017.11.06; Accepted: 2018.03.01; Published: 2018.04.09

Abstract

Rationale: Intravital optical imaging is a significant method for investigating cerebrovascular structure and function. However, its imaging contrast and depth are limited by the turbid skull. Tissue optical clearing has a great potential for solving this problem. Our goal was to develop a transparent skull window, without performing a craniotomy, for use in assessing cerebrovascular structure and function.

Methods: Skull optical clearing agents were topically applied to the skulls of mice to create a transparent window within 15 min. The clearing efficacy, repeatability, and safety of the skull window were then investigated.

Results: Imaging through the optical clearing skull window enhanced both the contrast and the depth of intravital imaging. The skull window could be used on 2-8-month-old mice and could be expanded from regional to bi-hemispheric. In addition, the window could be repeatedly established without inducing observable inflammation and metabolic toxicity.

Conclusion: We successfully developed an easy-to-handle, large, switchable, and safe optical clearing skull window. Combined with various optical imaging techniques, cerebrovascular structure and function can be observed through this optical clearing skull window. Thus, it has the potential for use in basic research on the physiopathologic processes of cortical vessels.

Key words: *in vivo* skull optical clearing, *in vivo* optical imaging, laser speckle contrast imaging, hyperspectral imaging, cerebral blood flow (CBF), oxygen saturation (SO_2).

Introduction

Observing cortical vascular structure and evaluating its functions are critical to understanding not only normal brain physiology but also the association between the progression of microvascular dysfunction and neurodegeneration in various brain diseases [1-7]. Optical imaging technology provides powerful tools for *in vivo* high-resolution cerebrovascular imaging [2, 6, 8-12]. An increasingly popular tool for imaging the cerebrovascular structure of the mammalian cortex is two-photon laser scanning microscopy (TPLSM) [13]. Other techniques for assessing physiological parameters include laser speckle contrast imaging (LSCI) [6] and hyperspectral imaging (HSI) [14, 15], which are used for monitoring hemodynamic changes in CBF [6, 7] and SO_2 [14, 16, 17], respectively.

However, the turbidity of the intact skull is a barrier for noninvasive cerebral optical imaging. Several types of skull windows have been proposed to overcome this obstacle, including thinned-skull

cranial window [18], open-skull glass window [19] and polished and reinforced thinned skull window (PoRTs) [20]. These windows satisfy research requirements in certain cases but with limitations. For example, repeated imaging in a large area can hardly be performed with the thinned-skull cranial window; a craniotomy window will nearly inevitably induce cortical injuries and inflammation [21, 22]. As for PoRTs, the operation procedure to create the window is extremely complex. Certain new techniques have been proposed for cerebrovascular optical imaging, including three-photon imaging [9, 23], near-infrared cerebrovascular imaging [10, 24], and non-invasive transcranial optical vascular imaging (nTOVI) [25]. However, the information attained with these techniques is limited by their imaging modalities, and the equipment used is very expensive. Fortunately, tissue optical clearing technique provides us a new option for solving this problem [26].

In this work, we developed innovative skull optical clearing agents, termed USOCA, for establishing an optical clearing skull window via topical application on the skull. We investigated the efficacy of the optical clearing skull window with respect to enhancement of the imaging resolution and depth, its use on mice at different ages, the ability to adjust the skull window size from regional to bi-hemispheric, and the ability to repeat clearing over the short and long term. Furthermore, we tested the safety of this optical clearing skull window by *in vivo* monitoring microglia dynamics [27], detecting the activation of microglia cells and the expression of glial fibrillary acidic protein (GFAP) several days after window establishment [19-21], and testing the metabolic toxicity of USOCA [28-30].

Methods

Preparation of USOCA

USOCA consists of S1 and S2, both of which are transparent and colorless, as shown in **Figure 1A**. S1 is a saturated supernatant solution of 75% (vol/vol) ethanol (Sinopharm, China) and urea (Sinopharm, China) at 25 °C. To prepare S1, ethanol is slowly dropped into and mixed with urea. The mixture needs to be stirred constantly, then should stand for 15 min to let the urea fully dissolve, after which the supernatant is removed. The volume-mass ratio of ethanol and urea is about 10:3. S2 is a high-concentration sodium dodecylbenzenesulfonate (SDBS) solution that is prepared by mixing 0.7 M NaOH solution (Aladdin, China) with dodecyl-benzenesulfonic acid (DDBSA, Aladdin) at a volume-mass ratio of 24:5, and the pH is kept at 7.2-8. The refractive indices (RI) of S1 and S2 are 1.399 ± 0.003 and 1.367 ± 0.005, respectively. Both S1 and S2 need to be sealed and stored at ~25 °C. The shelf life of both is about 2 months as long as they are not contaminated. **Figure 1B** shows the preparation of S1 and S2.

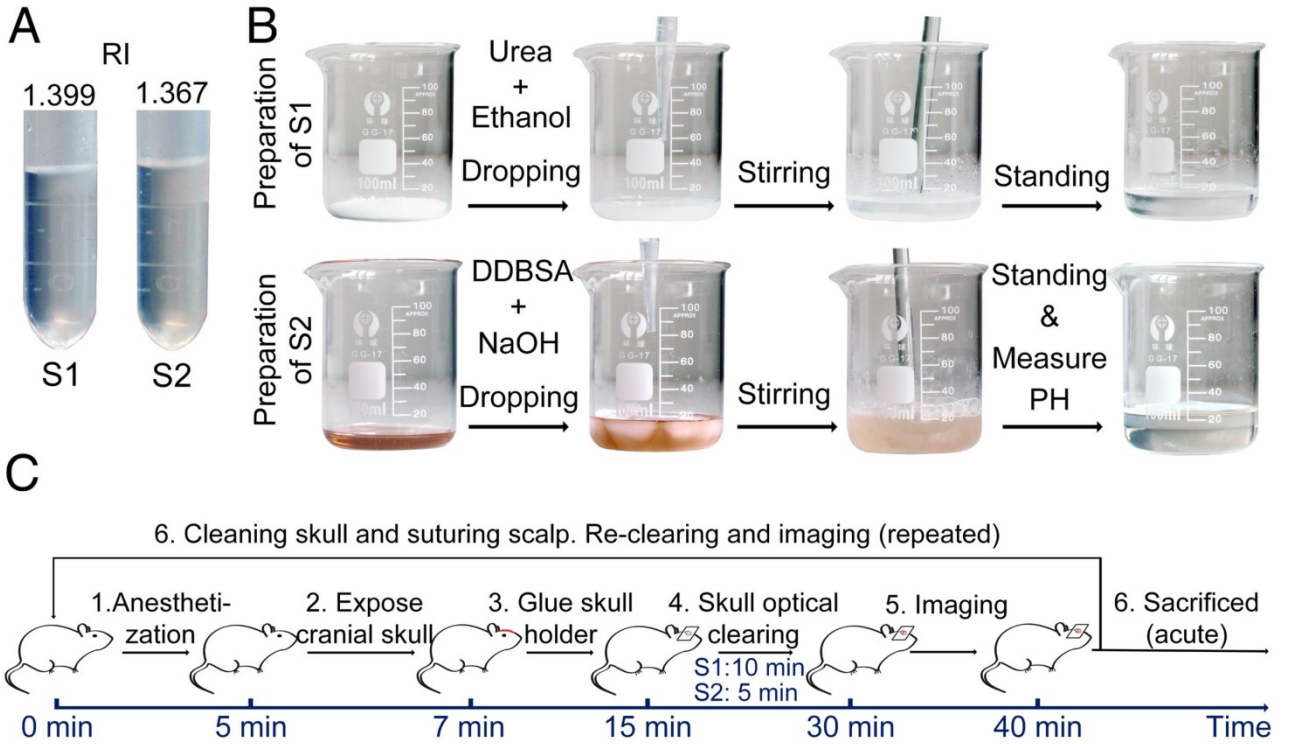

Figure 1. Preparation of USOCA and the experimental procedure. (A) Photograph of USOCA. **(B)** Steps of the preparation procedures for S1 and S2. **(C)** Steps in the experimental procedure.

Animal preparation and skull optical clearing procedure

All experimental protocols were performed according to the Experimental Animal Management Ordinance of Hubei Province, P. R. China, and the guidelines from the Huazhong University of Science and Technology, which have been approved by the Institutional Animal Ethics Committee of Huazhong University of Science and Technology. Unless stated otherwise, 2-month-old male BALB/c mice, supplied by Wuhan University Center for Animal Experiments (Wuhan, P. R. China), were used for the study. They were fed in specific pathogen-free (SPF) conditions.

The experimental procedure is shown in **Figure 1C**. First, mice were anesthetized with a cocktail of 2% α-chloralose and 10% urethane (8 mL/kg) via intraperitoneal injection. Second, the head of the mouse was shaved and a midline incision was made on the scalp along the direction of the sagittal suture. Third, mucosa on the skull was removed and the surface of the skull was dried using clean compressed air. Then, a holder was glued onto the skull (wide-field: H1; microscopic: H2 in **Figure S2**), and the mouse was immobilized in a custom-built plate [31]. Fourth, the skull optical clearing treatment was performed in two steps. S1 was applied to the exposed skull for about 10 min to allow the skull to gradually turn transparent. To accelerate the clearing, the skull was gently rubbed with a swab. Then, S1 was removed, and S2 was added to the same area for further clearing within 5 min. Generally, about 1 mL S1 and 0.3 mL S2 were needed to create a hemispheric optical clearing skull window. For a bi-hemispheric window, about 5 mL S1 and 1.5 mL S2 were needed. The treatment times for S1 and S2 have been optimized; occasionally the treatment time for S1 needs to be extended by 2-5 min for the skull to be effectively cleared. After creation of the optical clearing skull window, imaging was performed. What needs to be emphasized is that this optical clearing skull window is not permanent, and can be "closed" by scrubbing with phosphate-buffered saline (PBS, 0.01 M, Sigma-Aldrich, USA), drying and skin suturing.

Dual-modal optical imaging system combined LSCI with HSI for monitoring CBF and SO_2

LSCI and HSI were combined to create a dual-modal optical imaging system to monitor CBF and SO_2, respectively. A diagram of the system is shown in **Figure S3**. For LSCI, a He-Ne laser beam (λ=632.8 nm, 3 mW), expanded by a collimating lens, was used to illuminate the areas of interest. A CCD camera mounted on a stereomicroscope recorded a sequence of raw speckle images. For HSI, a ring-like LED light with a polarizer was used for illumination, and a liquid crystal tunable filter (LCTF, Perkin Elmer, USA) was placed in another channel of the stereo-microscope for splitting specific wavelengths. The hyperspectral signals were acquired by another CCD camera. Laser speckle temporal contrast [6] and multiple linear regression [8, 16] analysis methods were used to calculate CBF and SO_2, respectively.

The contrast-to-noise ratio (CNR), which was used to assess the imaging qualities of LSCI in some cases, was defined as [5, 29]:

$$\mathrm{CNR} = \frac{\left|C_{vessel} - C_{back}\right|}{\sqrt{f_{vessel}\sigma_{vessel}^2 + f_{back}\sigma_{back}^2}},$$

where C_{vessel} and C_{back} are the mean contrast values of the blood flow and the background, respectively; σ_{vessel}^2 and σ_{back}^2 are the variances in the contrast values of the blood flow and the background, respectively; and f_{vessel} and f_{back} are the fractions of pixels classified as blood flow and the background in all the selected pixels in the speckle contrast image, respectively.

TPLSM for assessing cerebrovascular microstructure

TPLSM (A1R MP, Nikon, Japan) was employed to image the cerebrovascular microstructure. The *NIS* software (Nikon, Japan) controlled the instrumentation during acquisition, processing, and storage of the image datasets. 100 μL tetramethylrhodamine-conjugated dextran (3 mg/mL, 70 kDa, Sigma-Aldrich, USA) was injected through the tail vein to mark the cerebral vessels. Mice (n=5) that underwent skull exposure and holder-mounting were placed on the experimental platform, and PBS was applied to the skull for imaging. PBS was then removed, and the skull was topically treated with USOCA. About 15 min later, a thin transparent polyethylene plastic film (thickness: 11±2 μm) was placed over the USOCA to separate USOCA from water. The fluorescence imaging of the same area was performed again.

Skull optical clearing efficacy for mice at different ages

The composition of the mouse skull changes with age [32, 33]. Therefore, we studied whether the optical clearing skull window was valid for mice at different ages. Male BALB/c mice aged 2, 4, 6 and 8 months (n=4 per age) were prepared in the same manner as outlined above and their cortical vessels were imaged using the LSCI/HSI imaging system in different conditions (skull intact, PBS- and USOCA-treated, and skull removed).

A large optical clearing skull window for monitoring cortical hemodynamics after middle cerebral artery occlusion (MCAO)

In this experiment, bi-hemispheric skulls of mice (n=4) were completely exposed and immobilized (by skull holder H3 in **Figure S2**), and the clearing process was the same as previously outlined. To obtain CBF and SO_2 maps of the bi-hemispheric cortex, images of the left, middle, and right sides were recorded in succession. The software *Image Composite Editor* (Microsoft, USA) was used to stitch the images together. Further, we investigated the bi-hemispheric cortical changes in CBF and SO_2 after MCAO. The surgical procedure used for MCAO was previously described [34].

Repeatability of the optical clearing skull window

An important property of an excellent optical imaging window is that it can be repeatedly created for constantly monitoring the dynamics of the cerebral vessels over a relatively long period. In this work, we repeatedly established the switchable optical clearing skull window and monitored the cortical vascular development in a short term (every other day for a week, n=5) and a long term (once a month for 6 months, n=4).

For each repeated experiment, the handling of the mice and the optical clearing procedure were performed as previously described. After each experimental trial, the skull holder was removed and the skull was completely cleaned with PBS, the incision was sutured, and antibiotic ointment was applied around the incision to prevent wound infection. Finally, the mice were placed on a heating pad until they revived and were placed in individual housing.

Safety of the optical clearing skull window

Safety is another important element by which to judge whether this skull window can be used in *in vivo* studies. We performed several *in vivo* and *in vitro* examinations to test the safety of the skull window, including exploring the activation of microglia cells, expression of GFAP, as well as metabolic toxicity.

To *in vivo* monitor microglia activation, 2-month-old male Cx3cr1-*GFP* mice (B6.129P-Cx3cr1^{tm1Litt}/J, Jackson Laboratory, Bar Harbor, ME, USA; stock No. 005582, n=4) were used. Animal preparation and imaging were similar to those in TPLSM used for cerebrovascular imaging.

As with microglia activity reaching a maximum 2 days after a craniotomy [21], we detected microglia activation 2 days after establishment of the optical clearing skull window. 2-month-old male Cx3cr1-*GFP* mice were used here also, whose left side of skull was optically cleared for 15 min. Two days later, the mice were perfused and fixed by PBS and 4% paraformaldehyde (PFA, Sigma-Aldrich, USA), then the brain was taken out and placed into 4% PFA overnight for post-fixation. The brain was then sliced (100 μm) and imaged by confocal microscopy (Zeiss, Germany).

To detect GFAP expression, the same steps as outlined above were performed, except that the brain slices were immunohistochemically stained with anti-GFAP antibodies (Sigma-Aldrich, USA) and imaged by an upright microscope system (Nikon, Japan) 10 days after USOCA application.

To test the metabolic toxicity of USOCA, 40 male BALB/c mice (2 months old) were randomly divided into two groups, with the skulls of one group treated with PBS and those of the other group treated with USOCA for 15 min every day for the first 3 days. After 28 days, the mice were weighed and killed, different organs were removed and weighed, and the body weight and organ-to-body weight ratio of each mouse in the control and USOCA-treated groups were obtained. Additionally, the liver and kidney underwent hematoxylin and eosin (H&E) staining because they were the target organs for revealing reagent toxicity [35].

Statistical analysis

In this work, all data are expressed as mean ± standard error unless stated otherwise. Significant differences were analyzed using one-way analysis of variance test with SPSS (IBM, USA).

Results

Efficacy of optical clearing skull window: Direct viewing

The extinction coefficients of oxy- and deoxyhemoglobin at 550 nm are strong, making both arteries and veins visible. Therefore, we obtained white-light images at 550 nm to observe cortical vessels. **Figure 2** presents direct observations of cortical vascular structure under different conditions. Before clearing, no vessels could be observed through the turbid skull. However, after a 15 min treatment with USOCA, abundant cortical vessels were seen by the naked eye. After scrubbing with PBS and drying, the skull returned to its initial turbid state again. White-light images of the skull clearing by using USOCA taken at different times are presented in **Figure S1**, and the dynamic clearing and recovery procedures are shown in **Video S1**. Repeated treatment with USOCA permitted us to establish the optical clearing skull window in the same area again,

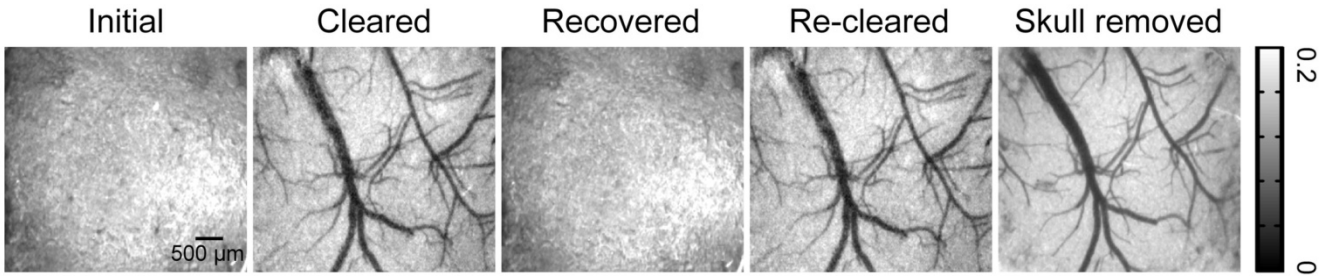

Figure 2. Typical white-light maps (at 550 nm) of cortical vessels under different conditions.

with the clearing efficacy similar to that of the first time. Therefore, this optical clearing skull window is both efficient and switchable. Moreover, after removing the skull in the window area, the cortical vascular structure seen was the same as that observed through the optical clearing skull window, whereby large vessels and microvessels were clearly distinguished in both situations.

Efficacy of optical clearing skull window: Enhanced cerebrovascular imaging depth

TPLSM was used to evaluate the enhancement of the cerebrovascular imaging depth based on the optical clearing skull window, as shown in **Figure 3**. We selected the same locations in the maximum intensity projection (MIP) maps and plotted the signal intensity profile along the dotted lines seen in **Figure 3**. The result showed that the signal intensity was enhanced greatly after clearing. The *z*-axis average signal intensity maps indicated that the imaging depth was also greatly enhanced. We randomly selected several microvessels (n=6) and calculated their diameters to determine the minimum resolvable vascular diameter before and after clearing. Before clearing, the imaging depth was about 120 μm, and only a few vessels (67.5 ± 7.9 μm) could be barely detected. However, with the optical clearing skull window, the imaging depth increased to about 300 μm, and both those large vessels and micro vessels (4.5 ± 0.31 μm) could be distinguished. These results suggest that the optical clearing skull window not only enhances imaging resolution and contrast but also improves imaging depth.

Efficacy of optical clearing skull window: Valid for mice at different ages

The composition of mouse skull changes with age [32, 33], so we evaluated the efficacy of USOCA on 2, 4, 6, and 8-month-old mice. **Figures 4A-D** present typical white-light (550 nm), SO_2, and CBF maps of cortical vessels for mice at 2, 4, 6, and 8 months of age, respectively. Cortical vessels were not visible on the white-light and SO_2 maps of the untreated skull. Although laser speckle temporal contrast analyzing method could provide some blurry information in the CBF map, the contrast and resolution were too low to distinguish cortical vessels clearly. When PBS was applied on the skull, the imaging quality slightly improved for the 2- and 4-month-old mice but not for the 6- and 8-month-old mice. However, with the application of USOCA, abundant cortical vessels were clearly observed, and the contrast and resolution of the CBF and SO_2 maps were greatly enhanced and were almost comparable to those obtained in all four age groups with the skull removal.

Next, we quantitatively analyzed CNR and minimum resolvable vascular diameter based on CBF images to evaluate image qualities; the results are shown in **Figures 4E-F**. There were significant differences in the CNR and the minimum resolvable vascular diameter between the PBS- and USOCA-treated groups in all age groups, implying that USOCA effectively enhanced image qualities. In addition, a comparison of these two parameters for the USOCA-treated and the skull-removed groups showed that there was a significant difference in the CNR for the 6- and 8-month-old mice (**Figure 4E**) but no significant difference in the minimum resolvable vascular diameter for mice of all ages (**Figure 4F**).

Skull removal was always accompanied by bleeding from the dura mater (indicated by yellow arrows in **Figure 4A-B, D**) and sometimes by the phenomenon of "lost" vessels (indicated by red arrows in **Figure 4B-C**), which would affect the imaging qualities and cause the loss of key information.

Efficacy of optical clearing skull window: Large window for monitoring bi-hemispheric hemodynamics after MCAO

Since our optical clearing skull window is established via topical application of USOCA to the skull, it can be enlarged from hemispheric to bi-hemispheric skull. We combined the large optical clearing skull window with LSCI/HSI and monitored the dynamic changes in CBF and SO_2 of bi-hemispheric cortex after MCAO surgery (**Figure 5**).

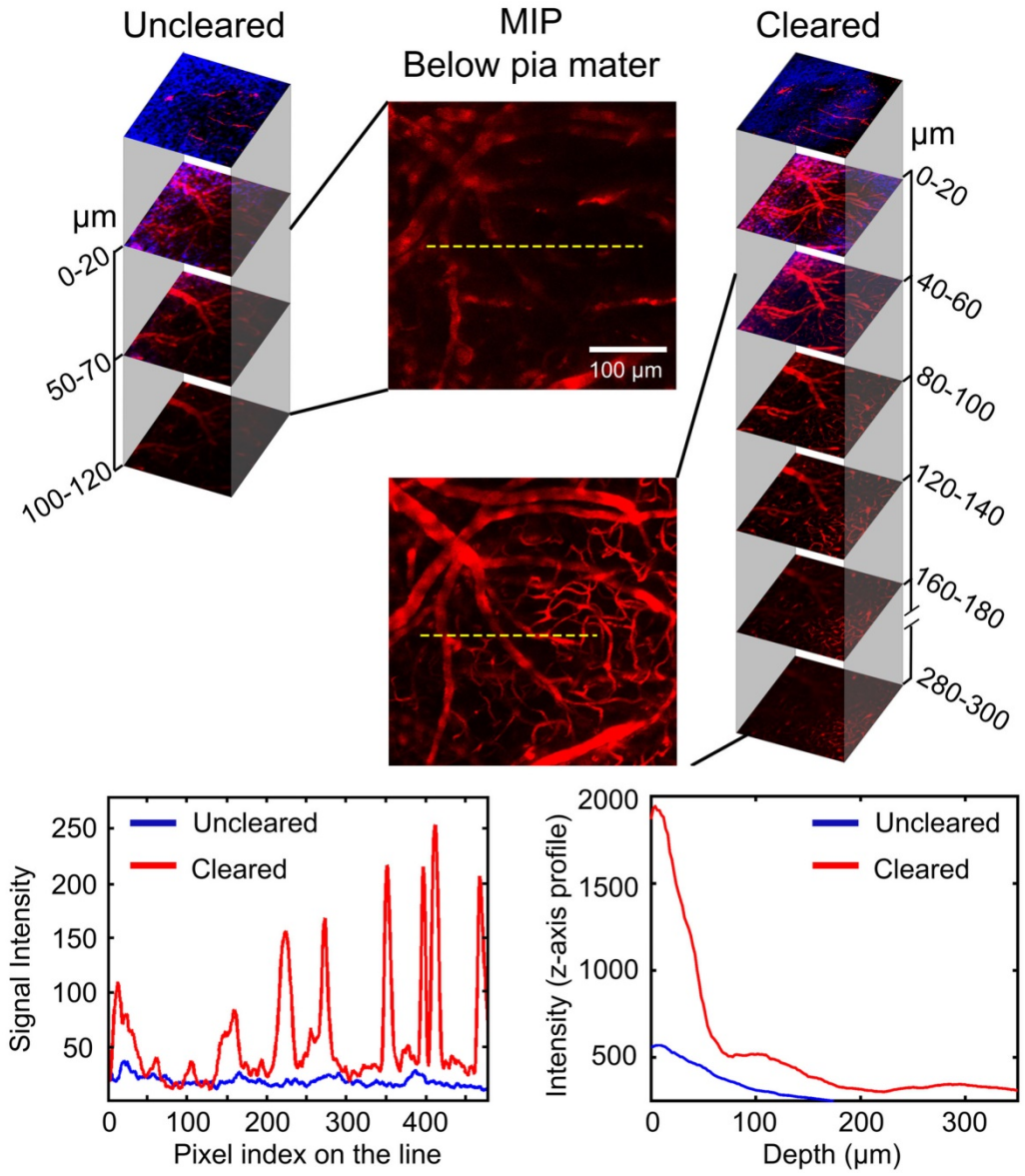

Figure 3. Evaluation of cerebrovascular imaging depth enhancement using the optical clearing skull window. Cortical vessels (red) and second harmonic generation (SHG) signals of skull (navy blue) at particular imaging depths were detected using TPLSM before and after clearing. MIP maps of cortical vessels below pia mater were obtained in the same area before and after clearing. Images (1024×1024 pixels, 0.78 μm/pixel) show maximum projections across 0-120 μm (uncleared) and 0-300 μm (cleared) below the pial surface; the z-step was 2 μm, the dwell time was 6.1 μs/pixel and the average power increased linearly from the top to the bottom (20-150 mW, excitation: 880 nm, detection: 595±25 nm, objective: 16×W 0.8 NA, zoom factor: 1). At the bottom, the left-hand plot is the signal intensity along the dashed lines in the MIP images. The right-hand plot is the signal intensity (z-axis profile) as a function of imaging depth before and after skull clearing.

With the establishment of the large optical clearing skull window, nearly all the cerebral blood vessels in bi-hemispheres were visible, and SO_2 and CBF of both hemispheres were obtained in **Figure 5Aa1-a3**. When MCAO surgery was performed on mice, we monitored the cortical hemodynamic changes induced by this acute ischemia. **Figure 5Aa4-a5** and **Figure 5Aa6-a7** are maps of SO_2 and CBF at 10 and 30 min after MCAO, respectively. Over time, both CBF and SO_2 at the surgery-operated side decreased radically; conversely, these two parameters increased at the opposite side. **Figures 5B-C** present the quantitative analysis of the relative changes in CBF and SO_2 of both arteries and veins at the surgery-operated side and the off-surgery side. CBF of the middle cerebral artery (MCA) on the operated side decreased ~60% of its initial value 10 min after MCAO surgery, and then dropped to ~0 at 30 min after MCAO (**Figure 5B**). In addition, CBF of the veins on the operated side decreased ~40% 10 min after surgery, and then decreased by ~60% of its initial value 30 min after surgery. Interestingly, the relative changes in SO_2 of both arteries and veins at the operated side were nearly the same as those in CBF in **Figure 5C**. At the opposite site, CBF increased dramatically. In arteries, CBF increased to almost three times of its initial value, and in veins, it increased by ~50% (**Figure 5B**). However, the SO_2 of

arteries and veins in the off-surgery side only increased slightly (**Figure 5C**).

Repeatability of optical clearing skull window: Short-term and long-term observation

Repeatability is an essential characteristic for an excellent skull window, because it allows the monitoring of structural and hemodynamic changes during the occurrence and development of some cerebrovascular diseases. We performed optical clearing in the same area of the skull every other day for 1 week (**Figure 6A**) or once a month as the mice aged from 2 to 7 months (**Figure 6B**), and obtained white-light, CBF, and SO_2 maps with each clearing.

Figure 6A shows that after each clearing, the skull became transparent so that abundant cortical vessels could be observed clearly. The cortical vascular structure as well as SO_2 and CBF remained stable during these clearings. The numbered peaks in the signal intensity plots, which show the signal intensity along the dash-dotted lines in the CBF images, correlate with the numbered vessels. The signal intensity values of the peaks were high enough so that each vessel could be distinguished after clearing, including small vessels such as 2 and 4 in **Figure 6A**.

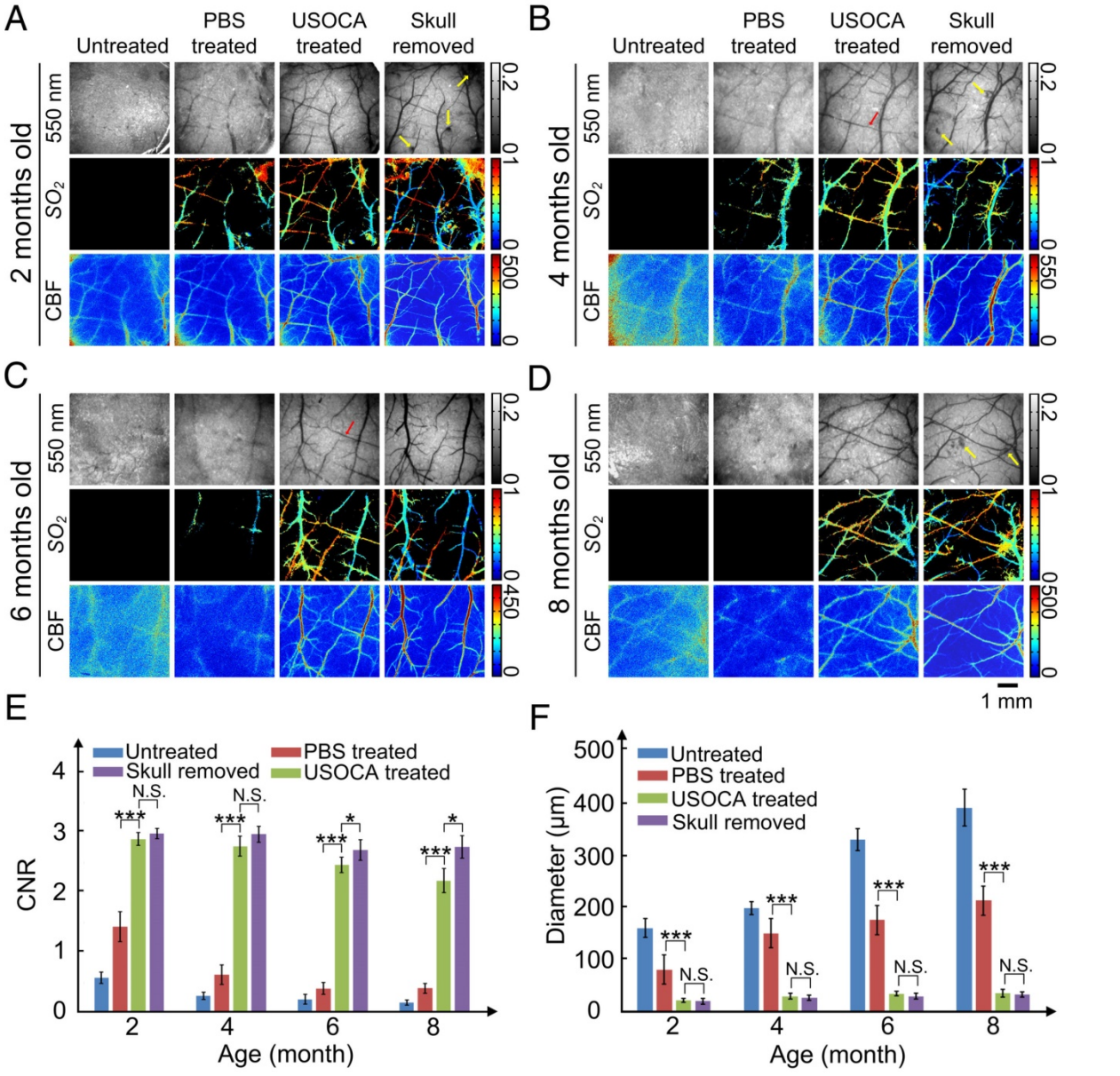

Figure 4. Establishment of optical clearing skull window on mice of different ages. (A-D) Typical white light, SO_2 and CBF images for mice at 2, 4, 6, 8 months of age, respectively. Yellow arrows indicate the bleeding areas of the dura mater caused by removal of the skull. Red arrow indicates the "lost" vessels after removing the skull. **(E)** CNR determined for mice at different ages and under different conditions based on LSCI images. *p<0.05, **p<0.01, ***p<0.001, and N.S.: no significant difference. **(F)** Bar graph of minimum resolvable vascular diameter for mice at different ages and under different conditions based on CBF images.

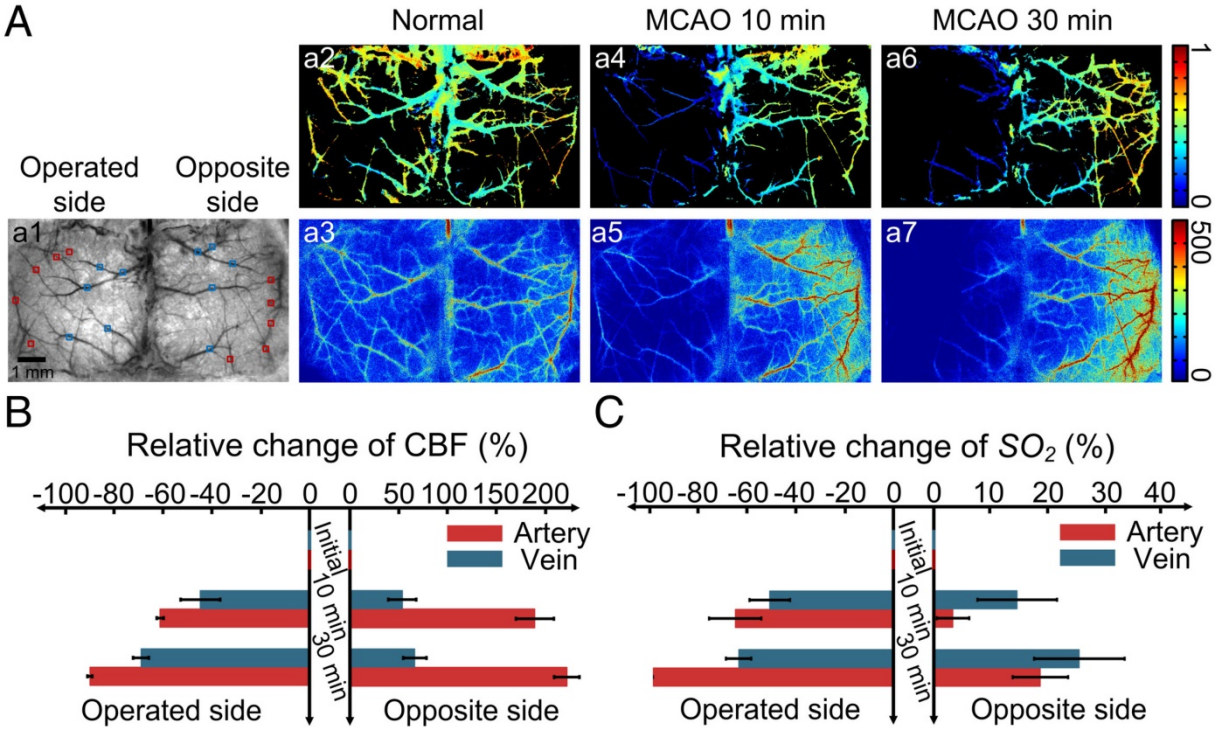

Figure 5. Establishment of a large optical clearing skull window over bi-hemispheres and monitoring the cortical hemodynamic changes induced by MCAO. (A, a1) White-light image of bi-hemispheric cortical vessels; rectangles are areas with arteries (red rectangles) and veins (blue rectangles) chosen for analysis. **(a2-a3)** SO_2 and CBF maps, respectively, of the bi-hemispheres in the normal state. **(a4-a5)** SO_2 and CBF maps, respectively, 10 min after MCAO. **(a6-a7)** SO_2 and CBF maps, respectively, 30 min after MCAO. **(B-C)** Bar graphs showing relative changes in SO_2 and CBF.

The long-term repeated clearing and imaging results presented in **Figure 6B** show that the optical clearing skull window was efficiently and repeatedly established once a month on mice as they aged from 2 to 7 months old. In addition, the vascular network was maintained relatively well, with only a few vessels appearing (V1) and "disappearing" (V2) (red and blue arrows in **Figure 6B**, respectively) over the 6 months, which was consistent with previous studies on cerebral angiogenesis [36].

Furthermore, we randomly selected a vein and an artery to find the change in their diameters induced by USOCA in repeated experiments over a short period (**Figure 6C**) and a long period (**Figure 6D**). Because images of each trial had some differences in angles and locations, we repeatedly calculated (5 times) their diameter to avoid artificial errors. Results suggested that neither arteries nor veins in short-term or long-term repeated experiments had significant differences, implying that repeatedly establishing the optical clearing skull window would not induce vascular distortion.

Safety of optical clearing skull window

We implemented several *in vivo* and *in vitro* examinations to further test the safety of optical clearing skull window, including *in vivo* monitoring of microglia dynamics in the resting state [27], detecting activation of microglia cells and expression of GFAP several days after optical clearing skull window establishment referring to the evaluation methods of other cranial windows safety [19-21], as well as H&E staining (liver and kidney) and organ to body weight ratio to reveal the metabolic toxicity of USOCA with methods commonly used to evaluate the effects of a chemical on health [28-30, 35].

After establishing the optical clearing skull window, we monitored the activation of microglia cells in the resting state for 1 h. Highly motile filopodia-like protrusions were clearly observed through the window (**Figure 7A**). In this process, the size, shape, and location of somata remained stable, suggesting that the optical clearing skull window is safe with respect to the brain cortex of the mouse [27].

We also performed *in vitro* studies to investigate the safety of the clearing window with respect to other aspects of microglia activation. An optical clearing skull window was established on the left side of the skull, making the left hemisphere the experimental side, and the right hemisphere the control side. We conducted this test because one study suggested that although some injuries (e.g., craniotomy) affected one side of the brain, adverse reactions would not extend to and affect the microglia activation and GFAP expression in the other side of the brain [21]. Results showed that two days after skull optical clearing, microglia in the superficial layers had neither assumed amoeboid shapes nor

extension toward the pial surface (**Figure 7B**). The expression levels of GFAP were detected ten days after window establishment. The results indicated that the skull optical clearing operation would not cause obvious signs of increased expression of GFAP at these two sides (**Figure 7C**).

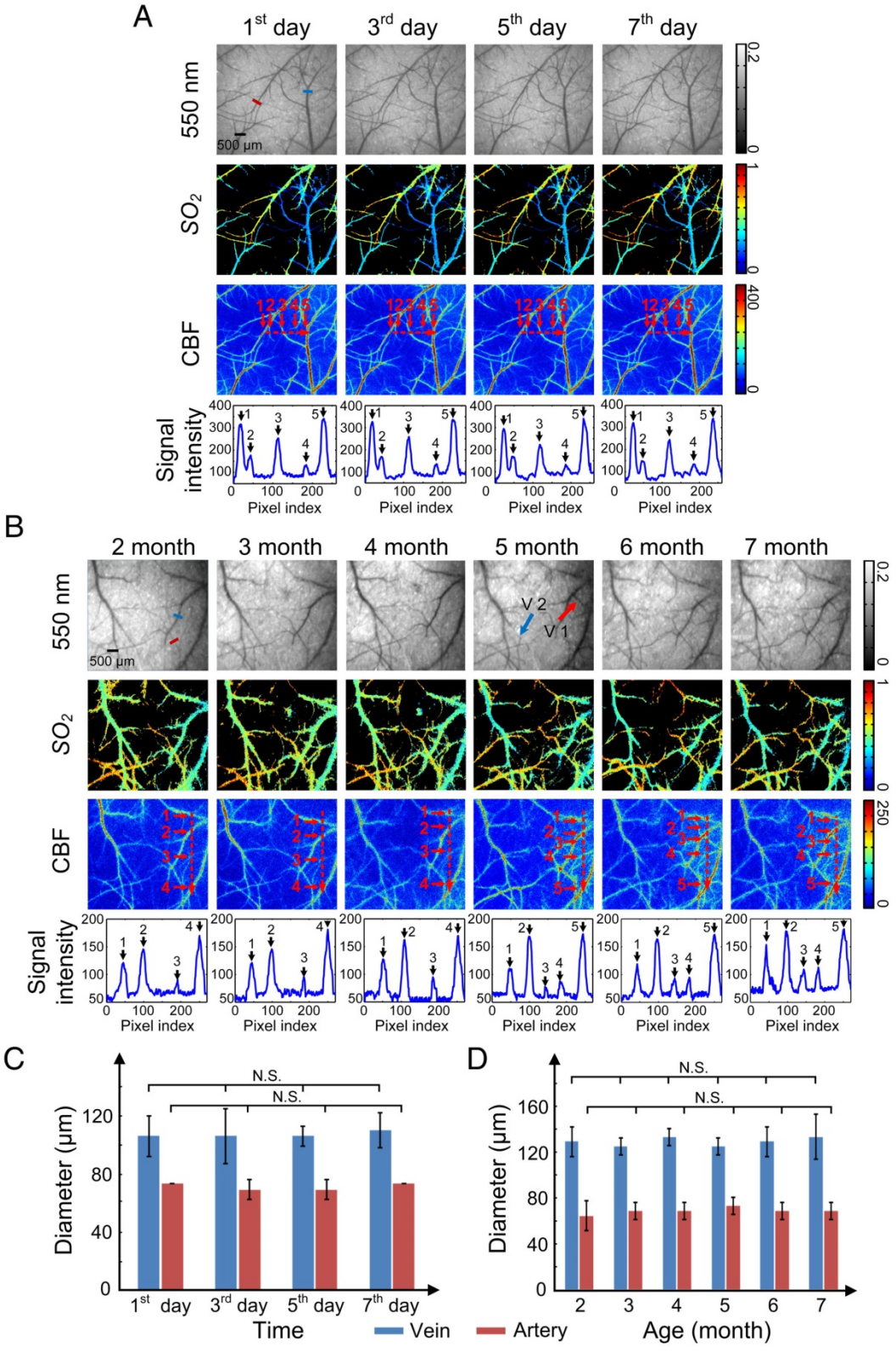

Figure 6. Repeatability of USOCA-based optical clearing skull window. (A) Optical clearing skull window was established every other day for 1 week on the same mouse to image cortical vessels. **(B)** Optical clearing skull window was established and cleared once a month over 6 months on the same mouse to image cortical vessels. Red and blue arrows indicate newly formed vessels and vessels that "disappeared", respectively. **(C)** Diameter of vein (blue short line in (A), top left panel) and artery (red short line in (A), top left panel) in short-term clearing. N.S.: no significant difference. **(D)** Diameter of vein (blue short line in (B), top left panel) and artery (red short line in (B), top left panel) in long-term clearing.

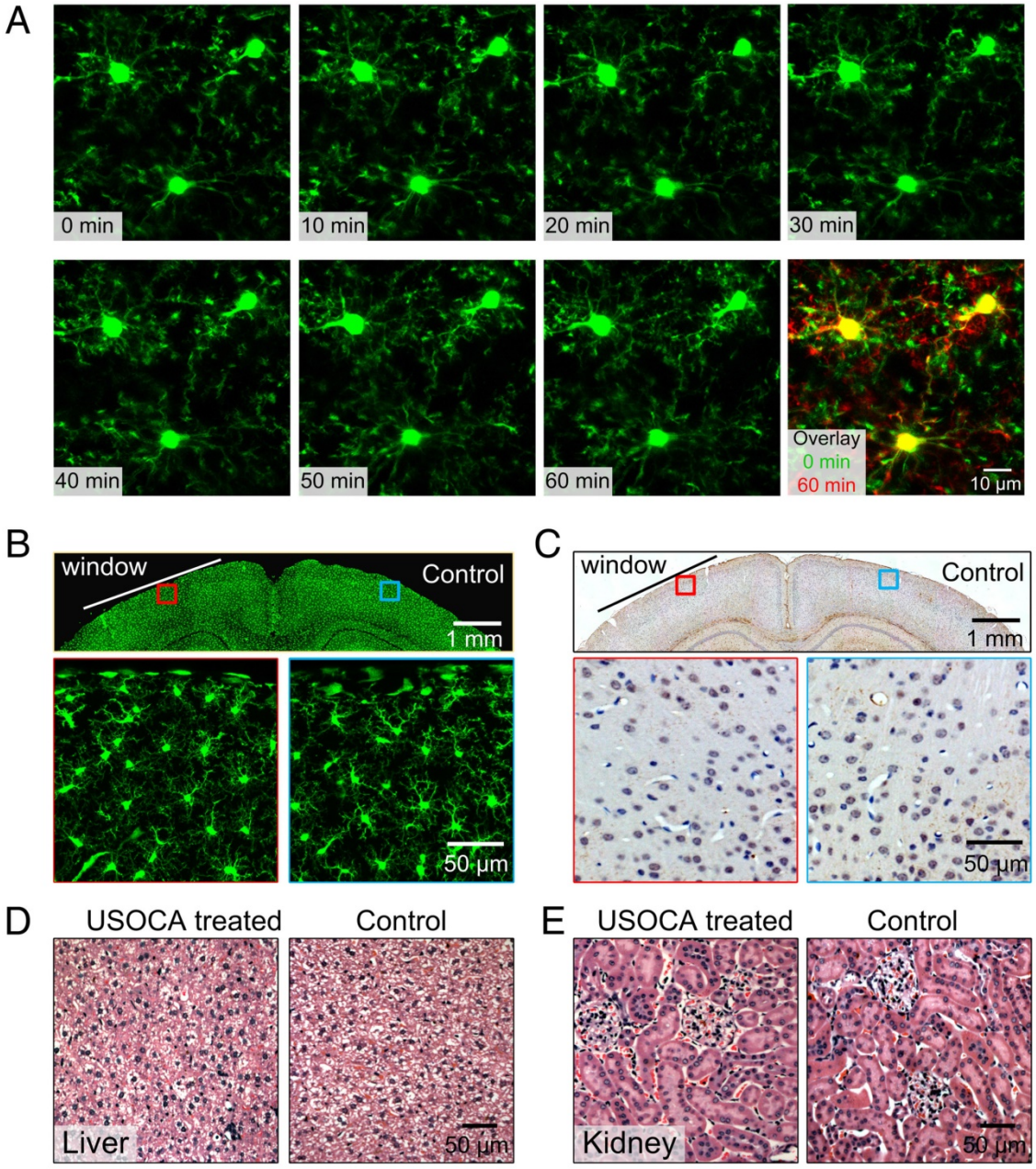

Figure 7. Safety evaluation of optical clearing skull window. (A) *In vivo* monitoring of microglia activation at 1 h. Images (1024×1024 pixels, 0.1 μm/pixel) show maximum projections across 30-70 μm below the pial surface; the z-step was 2 μm, the dwell time was 1 μs/pixel and the average power was 28 mW. (Excitation: 880 nm, detection: 525±25 nm, objective: 40× W 1.15 NA, zoom factor: 3). **(B)** Morphological changes in green fluorescent protein (GFP)-labeled microglia 2 days after skull optical clearing. The white line indicates the optical clearing skull window (diameter: 3-4 mm), and images in the second row are higher-magnification views of the red and blue boxed regions in the first row. **(C)** GFAP expression in astrocytes at the optical clearing skull window 10 days after skull optical clearing. The black line indicates the optical clearing skull window (diameter: 3-4 mm), and images in the second row are higher-magnification views of the red and blue boxed regions in the first row. **(D)** H&E staining (liver) of the experimental and control groups 28 days after establishment of the USOCA-based window. **(E)** H&E staining (kidney) of the experimental and control groups 28 days after establishment of the USOCA-based window.

Additionally, the H&E staining results in **Figures 7D-E** show that there are no obvious differences between slices of experimental and control groups, and no cellular aggregation or infiltration phenomena were present. In addition, the data in **Table S1** indicate that the body weights of the mice had not changed dramatically 28 days after a 3-day optical clearing treatment, and there was no significant difference between the control and experimental groups with respect to organ-to-body weight ratio. These collective results suggest that USOCA does not induce a pathological inflammatory response or metabolic toxicity in mice [19-21, 27-30].

Discussion

The results demonstrate that this efficient, large, switchable and safe optical clearing skull window permits monitoring of the cerebrovascular structure and cortical hemodynamics with satisfactory imaging resolution. Such monitoring is not achievable through

an intact turbid skull because of its complex composition and the refractive indices mismatch of the various components [26]. Several kinds of skull windows have been proposed for use in cortical imaging but have some limitations. Generally, researchers prefer to use a thinned-skull window in cerebrovascular studies because it satisfies requirements for instant imaging [18, 37]. However, the thinned-skull window is fragile and the skull needs to be re-polished before each imaging trial, thus, the imaging frequency is limited (usually no more than four times). Additionally, polishing the skull generates heat that can affect the cortical vessels, therefore, repeated skull polishing normally induces vascular proliferation and deformation [22, 38]. Open-skull glass window meets the requirement for long-term investigations, for example, it is applied to investigate cerebral angiogenesis [19, 39]. However, the imaging cannot be performed immediately after open-skull glass window establishment, because it takes approximately two weeks for mouse recovery and window stabilization. In addition, open-skull glass window sometimes damages cortical or dural vessels and induces inflammations [21, 22], therefore, it may cause misinterpretation of cerebral angiogenesis.

Tissue optical clearing is probably a better option. Recently, some *in vitro* tissue optical clearing methods have claimed that their chemical agents are efficient for clearing the skull [40-42]; however, their ingredients are biologically incompatible and toxic that will inevitably induce side effects for *in vivo* applications. And some intravital skull clearing agents have also been proposed, including a mixture of liquid paraffin and Vaseline [43] as well as SOCS [44, 45]. These methods have yielded some improvements in cortical imaging qualities, but their repeatability and safety have not been investigated. Therefore, we developed a new skull optical clearing method in this work. The skull optical clearing agent - USOCA, is comprised of S1 (a mixture of urea and ethanol) and S2 (high-concentration SDBS). Ethanol in S1 has a great potential in tissue optical clearing, because its hydroxyl group can contribute to form surface hydrogen bond bridges on the collagen triple helix to make collagen dissolution [46]. And urea is not only a common tissue optical clearing agent for its hydration effect, but also can greatly enhance the permeability of ethanol and accelerate clearance [47-49]. SDBS, as an ionic detergent, is used to extract lipids and make the skull uniform [50]. Under the actions of these chemical agents, the skull finally becomes transparent. By PBS scrubbing, the clearing agents are replaced, therefore, the skull recovers to its initial turbid status. To investigate the changes in collagen of skull, we measured the SHG signals (see **Figure S4**). A 10-min S1 treatment evidently reduced the SHG signal intensity and there were some cavities forming on the skull surface, which resulted from the collagen dissolution. With a 5-min S2 treatment, the SHG signal intensity seemed unchanged. After the skull was recovered by PBS scrubbing, the skull SHG signals had an enhancement and cavities were reduced. This indicated that the collagen might reassemble after recovery with PBS. Due to the complex nature of bone, the skull optical clearing mechanism needs to be further revealed.

This optical clearing skull window permits us to not only monitor cerebral blood flow and blood oxygenation by reflection imaging mode of LSCI and HSI, but also obtain fine cerebrovascular structure by TPLSM. In this work, we used the skull holders and holding plate (as shown in **Figure S2**) to immobilize the mouse, by this means, there was no observable movement of the skull induced by breathing and the heart beats of mice during the imaging procedure [18, 31]. Additionally, in two-photon imaging mode, a thin plastic film was used to separate water from clearing agent. To explore possible optical aberration in microscopic imaging caused by the refractive index mismatch among water, thin plastic film and clearing agent, we imaged 0.19 μm fluorescent beads (n=4) under three imaging conditions (water, water+plastic film, water+plastic film+USOCA-S2) (see **Figure S5**). The optical transfer function of two-photon-excited fluorescence measured through water and plastic film was modestly degraded compared to that measured through only water. But after applying S2, the resolution had a tiny improvement, with a radial width of ~0.5 μm (full width of half of the integrated intensity) and an axial resolution of ~2 μm. Overall, the refractive index mismatch among water, thin plastic film and clearing agent only causes a minimal effect on radial and axial resolutions.

Although the components of a mouse skull change with age, USOCA allows to efficiently establish the optical clearing skull window to observe cortical vessel structure and hemodynamics in mice from 2 to 8 months old. And the repeatability of our optical clearing skull window over a short and a long period was also verified. With long-term tracing, we observed that for the adult mouse, once the cerebrovascular network was established, it became a stable system that slowly regenerated. This is consistent with previous study [36]. Therefore, the proposed optical clearing skull window has a great potential in monitoring chronic brain disease processes.

Another advantage of this optical clearing skull window is that its size and location are adjustable.

Thus, it allows to investigate cortical activation in several brain regions simultaneously and establish the association between them. In this work, with the use of large optical clearing skull window, we observed bi-hemispheric hemodynamic changes after MCAO surgery. High-resolution imaging of the CBF and SO_2 distribution in both hemispheres allowed us to establish quantitative associations between the two hemispheres, which contributed to understand the mechanisms of brain lesions induced by MCAO.

Conclusions

In summary, an easy-to-handle, large, switchable, and safe optical clearing skull window was developed by topical application of USOCA. Combining with various optical imaging techniques, cerebrovascular structure and function could be observed with fine qualities. This optical clearing skull window was applicable to 2-8 months old mice, and satisfied the requirement for short- and long-term investigations about cortical blood flow and blood oxygen. Besides, the window size can be extended to bi-hemispheres, permitting us to monitor cortical hemodynamic changes in both hemispheres after MCAO. Additionally, USOCA was almost free of metabolic toxicity and the USOCA-based optical clearing skull window did not induce any cortical inflammations. We believe that combining this switchable optical clearing skull window with optical imaging techniques will contribute to *in vivo* tracing cortical vascular structural and functional changes towards the occurrence and development of some cerebrovascular diseases, which will be significant for evaluating the outcomes of some new therapeutics in future studies.

Abbreviations

CBF: cerebral blood flow; CNR: contrast-to-noise ratio; DDBSA: dodecylbenzenesulfonic acid; GFAP: glial fibrillary acidic protein; HSI: hyperspectral imaging; H&E: hematoxylin and eosin; LCTF: liquid crystal tunable filter; LSCI: laser speckle contrast imaging; MCA: middle cerebral artery; MCAO: middle cerebral artery occlusion; MIP: maximum intensity projection; nTOVI: transcranial optical vascular imaging; PBS: phosphate buffered saline; PFA: paraformaldehyde; PoRTs: polished and reinforced thinned skull window; RI: refractive indices; SDBS: sodium dodecyl benzene sulfonate; SHG: second harmonic generation; SO_2: oxygen saturation; SPF: specific pathogen free; TPLSM: two-photon laser scanning microscope.

Supplementary Material

Supplementary figures and tables.
http://www.thno.org/v08p2696s1.pdf

Video S1. http://www.thno.org/v08p2696s2.mp4

Acknowledgements

This work was supported by National Natural S cience Foundation of China (NSFC) (Grant Nos. 9123 2710, 31571002), the Foundation for Innovative Resear ch Groups of the National Natural Science Foundatio n of China (Grant No. 61721092), and Director Fund o f WNLO. We thank the Optical Bioimaging Core Facil ity of WNLO HUST for help with the imaging setup.

Competing Interests

The authors have declared that no competing interest exists.

References

1. Devor A, Sakadzic S, Srinivasan VJ, Ayaseen M, Nizar K, Saisan PA, et al. Frontiers in optical imaging of cerebral blood flow and metabolism. J Cerebr Blood F Met. 2012; 32: 1259-76.
2. Yao J, Wang L, Yang JM, Maslov KI, Wong TTW, Li L, et al. High-speed label-free functional photoacoustic microscopy of mouse brain in action. Nat Methods. 2015; 12: 407-13.
3. Wiesmann M, Zerbi V, Jansen D, Lutjohann D, Veltien A, Heerschap A, et al. Hypertension, cerebrovascular impairment, and cognitive decline in aged A beta PP/PS1 mice. Theranostics. 2017; 7: 1277-89.
4. Wiesmann M, Zinnhardt B, Reinhardt D, Eligehausen S, Wachsmuth L, Hermann S, et al. A specific dietary intervention to restore brain structure and function after ischemic stroke. Theranostics. 2017; 7: 493-512.
5. Murari K, Li N, Rege A, Jia X, All A, Thakor N. Contrast-enhanced imaging of cerebral vasculature with laser speckle. Appl Optics. 2007; 46: 5340-6.
6. Draijer M, Hondebrink E, Leeuwen T, Steenbergen W. Review of laser speckle contrast techniques for visualizing tissue perfusion. Laser Med Sci. 2009; 24: 639-51.
7. Shi R, Chen M, Tuchin VV, Zhu D. Accessing to arteriovenous blood flow dynamics response using combined laser speckle contrast imaging and skin optical clearing. Biomed Opt Express. 2015; 6: 1977-89.
8. Zuzak KJ, Schaeberle MD, Lewis EN, Levin IW. Visible reflectance hyperspectral imaging: Characterization of a noninvasive, in vivo system for determining tissue perfusion. Anal Chem. 2002; 74: 2021-8.
9. Horton NG, Wang K, Kobat D, Clark CG, Wise FW, Schaffer CB, et al. Three-photon microscopy of subcortical structures within an intact mouse brain. Nat Photonics. 2013; 7: 205-9.
10. Yue CX, Zhang CL, Alfranca G, Yang Y, Jiang XQ, Yang YM, et al. Near-Infrared Light Triggered ROS-activated Theranostic Platform based on Ce6-CPT-UCNPs for Simultaneous Fluorescence Imaging and Chemo-Photodynamic Combined Therapy. Theranostics. 2016; 6: 456-69.
11. Wang S, Lin J, Wang TF, Chen XY, Huang P. Recent Advances in Photoacoustic Imaging for Deep-Tissue Biomedical Applications. Theranostics. 2016; 6: 2394-413.
12. Huang YM, Lui H, Zhao JH, Wu ZG, Zeng HS. Precise Spatially Selective Photothermolysis Using Modulated Femtosecond Lasers and Real-time Multimodal Microscopy Monitoring. Theranostics. 2017; 7: 513-22.
13. Makino H, Ren C, Liu HX, Kim AN, Kondapaneni N, Liu X, et al. Transformation of Cortex-wide Emergent Properties during Motor Learning. Neuron. 2017; 94: 880-90.
14. Jeffcoate WJ, Clark DJ, Savic N, Rodmell PI, Hinchliffe RJ, Musgrove A, et al. Use of HSI to measure oxygen saturation in the lower limb and its correlation with healing of foot ulcers in diabetes. Diabetic Med. 2015; 32: 798-802.
15. Radrich K, Ntziachristos V. Quantitative multi-spectral oxygen saturation measurements independent of tissue optical properties. J Biophotonics. 2016; 9: 83-99.
16. Feng W, Shi R, Zhang C, Yu TT, Zhu D. Lookup-table-based inverse model for mapping oxygen concentration of cutaneous microvessels using hyperspectral imaging. Opt Express. 2017; 25: 3481-95.
17. Zhong XW, Wen X, Zhu D. Lookup-table-based inverse model for human skin reflectance spectroscopy: two-layered Monte Carlo simulations and experiments. Opt Express. 2014; 22: 1852-64.
18. Yang G, Pan F, Parkhurst CN, Grutzendler J, Gan WB. Thinned-skull cranial window technique for long-term imaging of the cortex in live mice. Nat Protoc. 2010; 5: 201-8.

19. Holtmaat A, Bonhoeffer T, Chow DK, Chuckowree J, De Paola V, Hofer SB, et al. Long-term, high-resolution imaging in the mouse neocortex through a chronic cranial window. Nat Protoc. 2009; 4: 1128-44.
20. Drew PJ, Shih AY, Driscoll JD, Knutsen PM, Blinder P, Davalos D, et al. Chronic optical access through a polished and reinforced thinned skull. Nat Methods. 2010; 7: 981-84.
21. Xu HT, Pan F, Yang G, Gan WB. Choice of cranial window type for in vivo imaging affects dendritic spine turnover in the cortex. Nat Neurosci. 2007; 10: 549-51.
22. Dorand RD, Barkauskas DS, Evans TA, Petrosiute A, Huang AY. Comparison of intravital thinned skull and cranial window approaches to study CNS immunobiology in the mouse cortex. Intravital. 2014; 3: e29728.
23. Ouzounov DG, Wang TY, Wang MR, Feng DD, Horton NG, Cruz-Hernandez JC, et al. In vivo three-photon imaging of activity of GCaMP6-labeled neurons deep in intact mouse brain. Nat Methods. 2017; 14: 388-92.
24. Hong GS, Diao S, Chang JL, Antaris AL, Chen CX, Zhang B, et al. Through-skull fluorescence imaging of the brain in a new near-infrared window. Nat Photonics. 2014; 8: 723-30.
25. Kalchenko V, Israeli D, Kuznetsov Y, Harmelin A. Transcranial optical vascular imaging (TOVI) of cortical hemodynamics in mouse brain. Sci Rep. 2014; 4: 5839.
26. Zhu D, Larin KV, Luo QM, Tuchin VV. Recent progress in tissue optical clearing. Laser Photonics Rev. 2013; 7: 732-57.
27. Nimmerjahn A, Kirchhoff F, Helmchen F. Resting microglial cells are highly dynamic surveillants of brain parenchyma in vivo. Science. 2005; 308: 1314-8.
28. Wang J, Shi R, Zhu D. Switchable skin window induced by optical clearing method for dermal blood flow imaging. J Biomed Opt. 2013; 18: 061209.
29. Wang J, Zhang Y, Li PC, Luo QM, Zhu D. Review: Tissue Optical Clearing Window for Blood Flow Monitoring. Ieee J Sel Top Quant. 2014; 20: 92-103.
30. Pal S, Chatterjee AK. Prospective protective role of melatonin against arsenic-induced metabolic toxicity in Wistar rats. Toxicol. 2005; 208: 25-33.
31. Yu X, Zuo Y. Two-Photon in vivo Imaging of Dendritic Spines in the Mouse Cortex Using a Thinned-skull Preparation. Jove-J Vis Exp. 2014; 87: e51520.
32. Gefen A, Gefen N, Zhu QL, Raghupathi R, Margulies SS. Age-dependent changes in material properties of the brain and braincase of the rat. J Neurotraum. 2003; 20: 1163-77.
33. Massie HR, Aiello VR, Shumway ME, Armstrong T. Calcium, iron, copper, boron, collagen, and density changes in bone with aging in C57BL/6J male mice. Exp gerontol. 1990; 25: 469-81.
34. Engel O, Kolodziej S, Dirnagl U, Prinz V. Modeling Stroke in Mice - Middle Cerebral Artery Occlusion with the Filament Model. Jove-J Vis Exp. 2011; 47: e2423.
35. Zhang LJ, Mu XQ, Fu JL, Zhou ZC. In vitro cytotoxicity assay with selected chemicals using human cells to predict target-organ toxicity of liver and kidney. Toxicology in Vitro. 2007; 21: 734-40.
36. Ina MWS, Fabian TS, Karl HP. Cerebral Angiogenesis During Development: Who Is Conducting the Orchestra? In: Milner R, ed. Cerebral Angiogenesis: Methods and Protocols. New York: Humana Press; 2014: 3-20.
37. Szu JI, Eberle MM, Reynolds CL, Hsu MS, Wang Y, Oh CM, et al. Thinned-skull Cortical Window Technique for In Vivo Optical Coherence Tomography Imaging. Jove-J Vis Exp. 2012; 69: e50053.
38. Rege A, Seifert AC, Schlattman D, Ouyang Y, Li KW, Basaldella L, et al. Longitudinal in vivo monitoring of rodent glioma models through thinned skull using laser speckle contrast imaging. J Biomed Opt. 2012; 17: 421-33.
39. Schrandt CJ, Kazmi SMS, Jones TA, Dunn AK. Chronic monitoring of vascular progression after ischemic stroke using multiexposure speckle imaging and two-photon fluorescence microscopy. J Cerebr Blood F Met. 2015; 35: 933-42.
40. Ke MT, Fujimoto S, Imai T. SeeDB: a simple and morphology-preserving optical clearing agent for neuronal circuit reconstruction. Nat Neurosci. 2013; 16: 1154-61.
41. Berke IM, Miola JP, David MA, Smith MK, Price C. Seeing through Musculoskeletal Tissues: Improving In Situ Imaging of Bone and the Lacunar Canalicular System through Optical Clearing. PloS One. 2016; 11: e0150268.
42. Greenbaum A, Chan KY, Dobreva T, Brown D, Balani DH, Boyce R, et al. Bone CLARITY: Clearing, imaging, and computational analysis of osteoprogenitors within intact bone marrow. Sci Transl Med. 2017; 9: eaah6518.
43. Tohmi M, Kitaura H, Komagata S, Kudoh M, Shibuki K. Enduring critical period plasticity visualized by transcranial flavoprotein imaging in mouse primary visual cortex. J Neurosci. 2006; 26: 11775-85.
44. Wang J, Zhang Y, Xu TH, Luo QM, Zhu D. An innovative transparent cranial window based on skull optical clearing. Laser Phys Lett. 2012; 9: 469-73.
45. Zhang Y, Zhang C, Zhong XW, Zhu D. Quantitative evaluation of SOCS-induced optical clearing efficiency of skull. Quant Imag Med Surg. 2015; 5: 136-42.
46. Hirshburg JM, Ravikumar KM, Hwang W, Yeh AT. Molecular basis for optical clearing of collagenous tissues. J Biomed Opt. 2010; 15: 055002.
47. Chen L, Li G, Li Y, Li Y, Zhu H, Tang L, et al. UbasM: An effective balanced optical clearing method for intact biomedical imaging. Sci Rep. 2017; 7: 12218.
48. Tainaka K, Kuno A, Kubota SI, Murakami T, Ueda HR. Chemical Principles in Tissue Clearing and Staining Protocols for Whole-Body Cell Profiling. Annu Rev Cell Dev B, 2016; 32: 713-41.
49. Hama H, Kurokawa H, Kawano H, Ando R, Shimogori T, Noda H, et al. Scale: a chemical approach for fluorescence imaging and reconstruction of transparent mouse brain. Nat Neurosci. 2011; 14: 1481-1488.
50. Yang B, Treweek JB, Kulkarni RP, Deverman BE, Chen CK, Lubeck E, et al. Single-Cell Phenotyping within Transparent Intact Tissue through Whole-Body Clearing. Cell. 2014; 158: 945-58.